Electronic Supplementary Material (ESI) for Journal of Materials Chemistry A.

Supporting Information

VANADIUM PENTOXIDE / CARBIDE-DERIVED CARBON CORE-SHELL HYBRID PARTICLES FOR HIGH PERFORMANCE ELECTROCHEMICAL ENERGY STORAGE

Marco Zeiger,[1,2] Teguh Ariyanto,[3] Benjamin Krüner,[1,2] Nicolas J. Peter,[4] Simon Fleischmann,[2]

Bastian J. M. Etzold,[3,5,] and Volker Presser[1,2,*]*

[1] *INM - Leibniz Institute for New Materials, 66123 Saarbrücken, Germany*

[2] *Department of Materials Science and Engineering, Saarland University, 66123 Saarbrücken, Germany*

[3] *Friedrich-Alexander Universität Erlangen-Nürnberg, Lehrstuhl für Chemische Reaktionstechnik, 91058 Erlangen, Germany*

[4] *Max-Planck Institut für Eisenforschung GmbH, 40237 Düsseldorf, Germany*

[5] *Technische Universität Darmstadt, Ernst-Berl-Institut für Technische und Makromolekulare Chemie, 64287 Darmstadt, Germany*

* *Corresponding authors. Bastian Etzold:* etzold@tc1.tu-darmstadt.de. *Volker Presser:* volker.presser@leibniz-inm.de

Elemental mapping with EF-TEM

The vanadium post-edge window ranged from 523-533 eV, while the oxygen post-edge window ranged from 534-544 eV. Thereby, both the major white lines of the vanadium and the two peaks of the oxygen K-edge were captured separately. Each image of an energy-filtered map was taken with an exposure time of 40 s in case of carbon and 60 s of vanadium and oxygen. The background was fitted from the two pre-edge images with a power law function. The two pre-edge and one post-edge image were automatically taken in Digital Micrograph (Gatan) to form one elemental map. Cross-correlation was applied to account for sample drift between the images acquired in a three-window series. In addition, the three separately obtained elemental maps of carbon, vanadium and oxygen were aligned using a cross-correlation to ensure a proper spatial superposition of the individual RGB channels. Oxygen is shown in green, vanadium in blue and carbon in red to finally form the multi-component elemental distribution map. The reference TEM image of the exact same area of the elemental distribution map was acquired using mainly the elastically scattered electrons by centering an energy selecting slit with a width of 10 eV around the zero loss peak to increase the contrast in the image. The corresponding thickness map, for which an additional unfiltered image without slit was captured, revealed relative thicknesses t/λ (in units of λ, the material-dependent mean free path for inelastic scattering) ranging from 0.1 to about 1.5.

Thermogravimetric analysis

In **Figure S1** the results of the annealing process in synthetic air of all VC/CDC samples as well as the VC precursor are shown. The calcination of VC to V_2O_5 starts at ~375 °C. At ~600 °C the transformation is complete with a mass gain of ~40 mass%. As expected the same procedures completely burns off the CDC. A suitable temperature between 375 °C and 600 °C is 450 °C which was used for the synthesis of V_2O_5/CDC. At 450 °C for 30 min the VC reaches a mass gain of ~40 mass% similar to the annealing procedure with a maximum temperature of 600 °C accompanied by a phase transformation from VC to V_2O_5. The pure carbon sample VC-CDC loses around 20 mass%. Partially etched VC samples with porous carbon shell and VC core presents slightly smaller mass loss due to the remaining carbon shell.

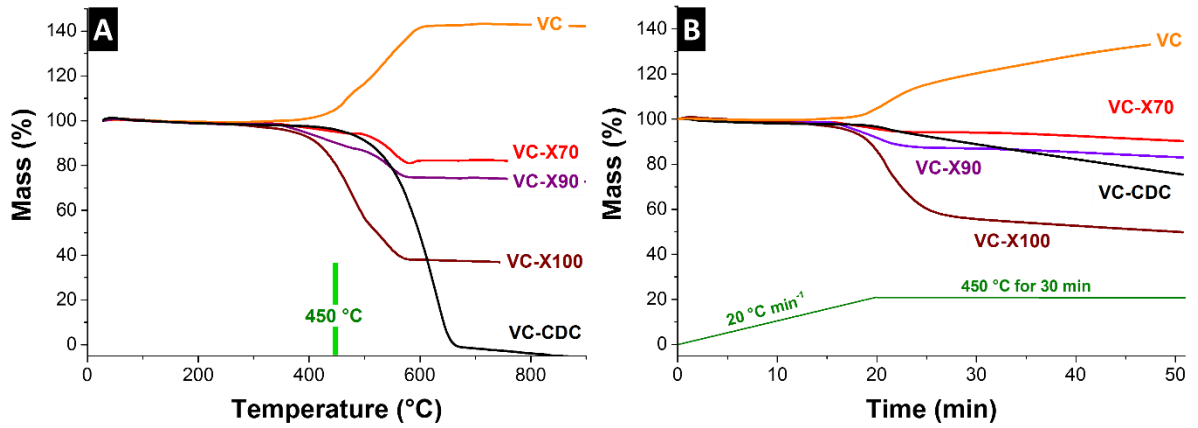

Figure S1: Thermogravimetric analysis in synthetic air with a heating rate of 20 °C·min^{-1} (A) until 900 °C and (B) until 450 °C and holding for 30 min.

X-ray diffraction

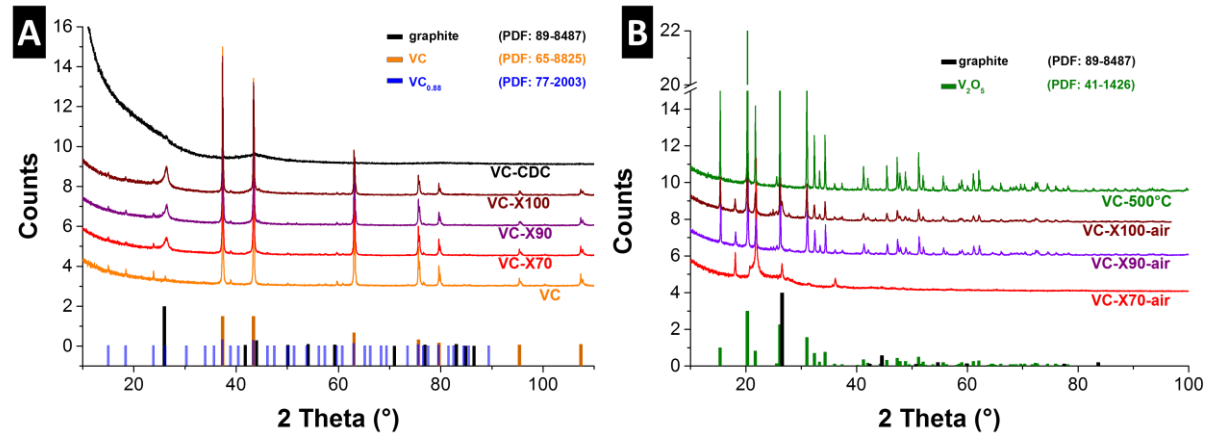

Figure S2: X-ray diffractogramms of VC/CDC composites (A) and V_2O_5/CDC composites (B).

Nitrogen gas sorption analysis

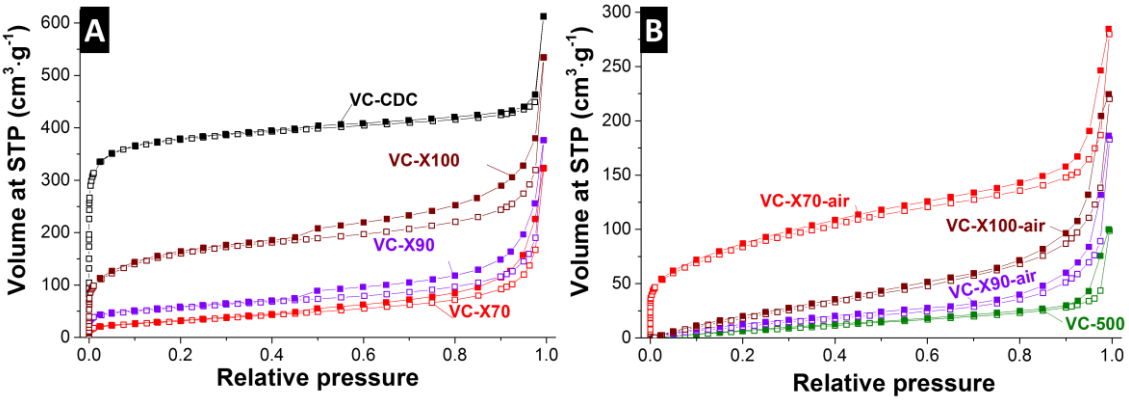

Figure S3: Nitrogen sorption isotherms of VC/CDC composites (A) and V_2O_5/CDC composites (B).

Electrochemical measurements

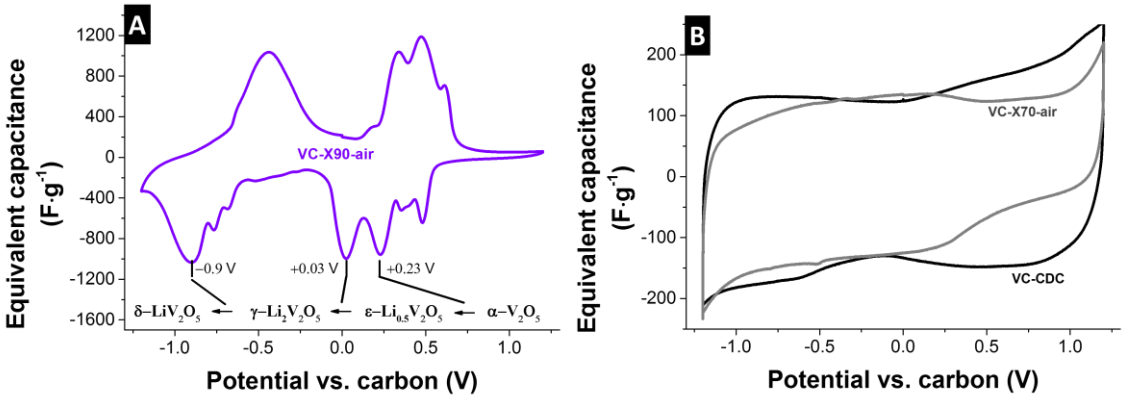

Figure S4: Cyclic voltammograms of VC-X90-air (A) and VC-X70-air and VC-CDC (B) at 1 $mV \cdot s^{-1}$ in half cell configuration.

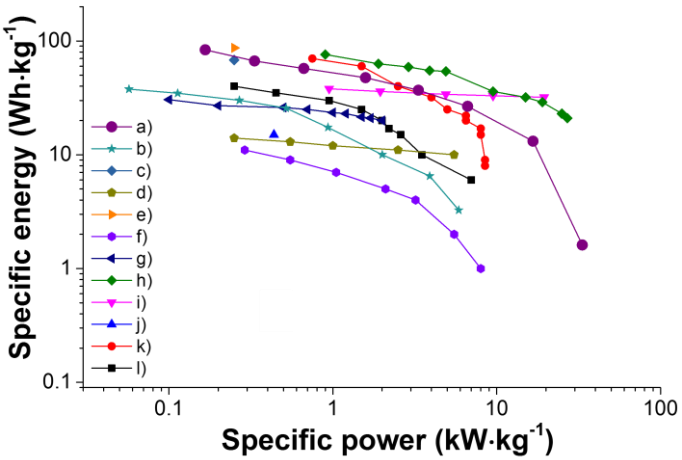

Figure S5: Ragone plot. a) this study, b)[1], c)[2], d)[3] e)[4], f)[5], g)[6], h)[7], i)[8], j)[9], k)[10].

Scanning electron micrographs

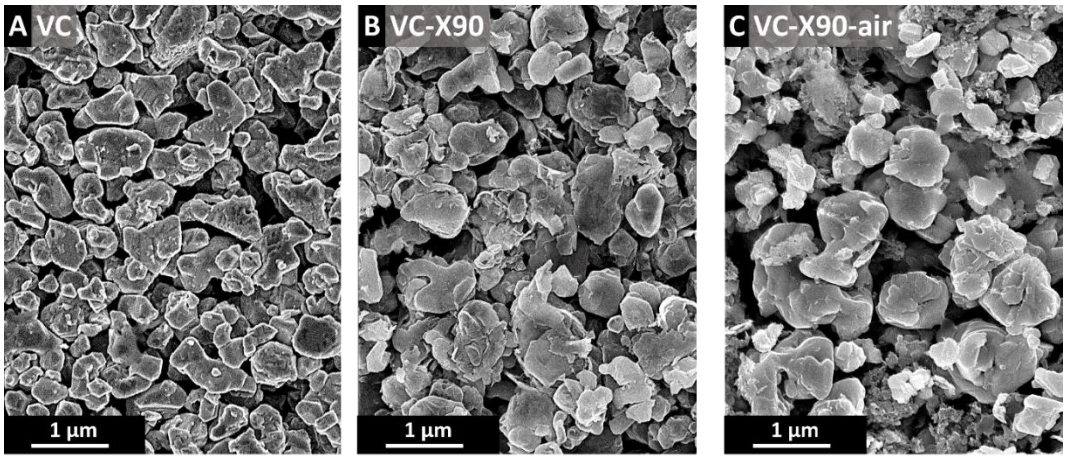

Figure S6: Scanning electron micrographs of (A) VC, (B) VC-X90, and (C) VC-X90-air.

Electrode conductivity measured using 4-point probe

Table S1: Electrode conductivity measured using 4-point probe. "n.d." means not detectable and related to values which are below the detection limit of the system.

	Electrode conductivity $S \cdot cm^{-1}$
VC-CDC	0.54±0.02
VC-X70-air	0.12±0.03
VC-X90-air	0.14±0.05
VC-X100-air	0.13±0.03
VC-500 pure	n.d.
VC-500 (25mass% VC-CDC)	0.05±0.01

Supporting references

1. S. Fleischmann, N. Jäckel, M. Zeiger, B. Krüner, I. Grobelsek, P. Formanek, S. Choudhury, D. Weingarth and V. Presser, *Chemistry of Materials*, 2016, **28**, 2802-2813..
2. Y. Wu, G. Gao and G. Wu, *Journal of Materials Chemistry A*, 2015, **3**, 1828-1832.
3. T. Qian, N. Xu, J. Zhou, T. Yang, X. Liu, X. Shen, J. Liang and C. Yan, *Journal of Materials Chemistry A*, 2015, **3**, 488-493.
4. Y. Wu, G. Gao, H. Yang, W. Bi, X. Liang, Y. Zhang, G. Zhang and G. Wu, *Journal of Materials Chemistry A*, 2015, **3**, 15692-15699.
5. C. X. Guo, G. Yilmaz, S. Chen, S. Chen and X. Lu, *Nano Energy*, 2015, **12**, 76-87.
6. Q. T. Qu, Y. Shi, L. L. Li, W. L. Guo, Y. P. Wu, H. P. Zhang, S. Y. Guan and R. Holze, *Electrochemistry Communications*, 2009, **11**, 1325-1328.
7. D. H. Nagaraju, Q. Wang, P. Beaujuge and H. N. Alshareef, *Journal of Materials Chemistry A*, 2014, **2**, 17146-17152.
8. X. Zhou, Q. Chen, A. Wang, J. Xu, S. Wu and J. Shen, *ACS Applied Materials & Interfaces*, 2016, **8**, 3776-3783.
9. S. D. Perera, M. Rudolph, R. G. Mariano, N. Nijem, J. P. Ferraris, Y. J. Chabal and K. J. Balkus Jr, *Nano Energy*, 2013, **2**, 966-975.
10. S. D. Perera, B. Patel, N. Nijem, K. Roodenko, O. Seitz, J. P. Ferraris, Y. J. Chabal and K. J. Balkus, *Advanced Energy Materials*, 2011, **1**, 936-945.